Heliyon

Received:
2 August 2018
Revised:
19 January 2019
Accepted:
12 March 2019

Cite as: Niharika Nagar, Vijay Devra. A kinetic study on the degradation and biodegradability of silver nanoparticles catalyzed Methyl Orange and textile effluents.
Heliyon 5 (2019) e01356.
doi: 10.1016/j.heliyon.2019.e01356

A kinetic study on the degradation and biodegradability of silver nanoparticles catalyzed Methyl Orange and textile effluents

Niharika Nagar, Vijay Devra*

Department of Chemistry, J.D.B. Govt. P.G. Girls College, Kota, Rajasthan, 324001, India

* Corresponding author.

E-mail address: v_devra1@rediffmail.com (V. Devra).

Abstract

The present study includes the *Azadirachta indica* (neem) induced Silver nanoparticles (AgNPs) by green synthesis as reducing and capping agent. Synthesized AgNPs were characterized by different instrumental techniques such as XRD (X-ray Diffraction), SEM (Scanning Electron Microscopy), TEM (Transmission Electron Microscopy), Zetasizer, UV-Visible and FT-IR (Fourier Transformation Infra-Red) spectroscopy. The result of XRD reveals that nanoparticles were crystalline in nature and pure, stability was determined by Zeta potential and SEM, TEM analysis indicates that AgNPs was monodisperse in a spherical shape with average size 9 nm. These synthesized AgNPs were applied as the catalyst in the degradation process of Methyl Orange (MO) and wastewater samples in presence of peroxodisulphate (PDS). Effect of different experimental conditions such as initial pH, concentration of PDS, Dye, and AgNPs was studied on the degradation process. The obtained kinetic result shows that AgNPs/PDS system induces 1.1×10^{-4} to 15.9×10^{-4} s^{-1} folds in presence of the small concentration of AgNPs (1×10^{-8} mol dm^{-3}). The degradation of MO and real wastewater samples in AgNPs/PDS system is followed pseudo-first order kinetics and maximum degradation of MO reached

https://doi.org/10.1016/j.heliyon.2019.e01356

88% in 40 min and real wastewater samples in 80 min. Liquid chromatography-mass spectrometry (LC-MS) analysis and UV-Visible spectral changes were used to analyze the structure of intermediate and end products (CO_2, H_2O, NO_3^-, and O_3S^-) during the degradation process. Furthermore, the result of biodegradability index (greater than 0.3) implies that advanced oxidation process enhances the biodegradability of wastewater.

Keywords: Physical chemistry, Materials chemistry

1. Introduction

Water pollution due to the discharge of coloured effluents from textile dye manufacturing and textile dyeing mills are one of the major environmental concerns, in the world today. Strong colour imparted by the dyes to the receiving aquatic ecosystem poses aesthetic and serious ecological problems. Therefore numbers of techniques aimed at preferential removal dyes from wastewater have been developed such as adsorption [1, 2, 3, 4], ion exchange [5], membrane filtration [6]. However, these techniques have merely transferred the dye from one form of waste to another, thus generally secondary pollutants requiring further treatment [7]. In the past few decades, the advanced oxidation process has attracted extensive attention as innovative wastewater treatment technologies for the degradation of organic pollutants in less harmful products [8, 9, 10]. Some reactive oxidising species such as $^{\bullet}OH$, $O_2^{\bullet-}/HO_2^{\bullet-}$ can be generated in AOP and are usually very efficient for dye bleaching and even mineralization. Recently sulphate radical ($SO_4^{\bullet-}$) based AOP has attracted great scientific and technological interest in environmental application [11, 12, 13]. Sulphate radicals (SRs), with the reduction potential of +2.6 V vs NHE, can be produced by the activation of sulphate based oxidants (PMS, PDS) with heat, ultraviolet, microwave and ultrasound irradiation and/or transition metal ions. A series of experiments evidence has provided that silver nanoparticles (AgNPs) are the best catalyst for the activation of PDS to produce SRs for degradation of persistent organic pollutants in water [14, 15, 16].

Nanosized metal nanomaterials are drawing the devotion of present science field nanometer scale leads to particular intrinsic properties for the materials that render them very likely for application in catalysis [17, 18, 19, 20]. Inorganic nanoparticles exhibit unique physical and chemical characteristics, creation to the development of novel applications in catalysis [21, 22, 23, 24, 25]. Silver nanoparticles are widely used and known applications in medical and pharmaceutical products and are hence directly encountered by the human system. Recently, nanotechnology has been developed in dynamic disciplines of research in material science in which plants and plant products are finding in the application of synthesis of nanoparticles [26,

https://doi.org/10.1016/j.heliyon.2019.e01356

27, 28, 29]. Even though the medicinal importance of numerous plants was known, the plant-mediated silver nano-product is a relatively newer concept.

Although studies on the kinetics of oxidative degradation of dye with PDS have been widely carried out [30, 31], very few attempts have been made so far on the oxidative degradation of MO in presence of metal nanoparticles [32, 33, 34, 35]. However, in our best of knowledge from *Azadirachta indica* (neem), synthesized AgNPs has not yet been investigated in degradation of MO. Here we evaluated catalytic activity of green synthesized AgNPs in the oxidative degradation of MO by PDS in an aqueous medium. The present research work also includes the catalytic activity of AgNPs in dye-containing wastewater, collected from drains of local industries situated in Kota city, Rajasthan (India). The present work is based on excellent economy of the process in terms of cheaper chemicals, rapid and convenient green method. Moreover, the AgNPs/PDS system was also evaluated for biodegradability index of different samples.

2. Materials and method

2.1. Chemicals and materials

Silver nitrate ($AgNO_3$) (E. Merck), Peroxodisulfate ($K_2S_2O_8$) (Sigma−Aldrich), Methyl orange and other reagents including H_2SO_4, NaOH were of analytical grade. The plant *Azadirachta indica* (neem) was selected from Kota (Rajasthan) India, Fresh and healthy leaves of plant neem cleaned, dried and stirred on a magnetic stirrer at 80 °C for 20 min. The obtained neem extract was filtered, refrigerated (4 °C) for further experiments. Deionised water was employed throughout the study. The wastewater samples were collected from the different local textile industries of Kota city (Rajasthan, India).

2.2. Instrumentation

For kinetic measurements and estimation of AgNPs synthesis, a Peltier accessory (temperature-Controlled) attached to a UV-Visible double beam spectrophotometer (3000^+ LABINDIA) was used. Fourier Transformation Infra-Red (FTIR Model-ALPHA-T Bruker, Germany) analysis results give information about the functional group of the biomolecules present in the leaf broth of *Azadirachta Indica* (Neem). Transmission Electron Microscopy (TEM) (Model-Tecnai G^2 20 (FEI) S-Twin) and Scanning Electron Microscopy (SEM) (Model-Nova Nano FE-SEM 450 (FEI)) instrument were used for the morphological study of AgNPs. XRD analysis was done by using XPERT-PRO X-Ray Diffractometer of Cu K_α radiation ($\lambda = 0.1540$ nm) with a scanning rate of 2°/min and 2θ ranging from 10° to 89°. To check the stability and size of synthesized NPs were determined by Zetasizer ver. 7.11 Malvern. The LC-ESI-MS (Model- Q-TOF Micromass, WATERS Company, UK) was

https://doi.org/10.1016/j.heliyon.2019.e01356

used for analysis of degradation product and pH measured by pH meter (MSW-552). COD and BOD measurements determined according to the Winkler method with azide modification.

2.3. Synthesis of silver nanoparticles

For a synthesis, 10% neem leaf broth added in 20 ml of $AgNO_3$ (1×10^{-3} mol dm^{-3}) solution at 30 °C with continuous stirring at magnetic stirrer. Formation of nanoparticles was observed by UV-Visible spectra of the solution at different time and color change. The yellowish colloidal brown colour shows the complete reduction of Ag^+ ions into Ag° as described in our previous study [36]. Synthesized nanoparticles are stable for one month under ambient condition.

2.4. Kinetic measurements

The oxidative degradation of Methyl orange (MO) was carried out with the desired concentration of reactants in stoppered Erlenmeyer flask at 30 °C. The reaction was initiated by adding the known volume of PDS solution. The kinetics was monitored by the absorbance of MO measured spectrophotometrically at λ_{max} 465 nm in a regular time interval. It was observed that the absorbance (A) of the dye solution decreases with increasing time showing the progress of dye degradation. Beer's law was obeyed at 465 nm over the concentration range (1×10^{-5} to 1×10^{-4} mol dm^{-3}); the molar absorptivity index of MO was found to be 24570 ± 50 mol^{-1} dm^3 cm^{-1} [37]. The degradation of real dye-containing wastewater samples was also carried out in presence of AgNPs. The degradation of dye sample was measured spectrophotometrically at λ_{max} 438, 445, 480 nm in a regular time interval. A plot of $2 + \log$ (A) versus time was found linear which indicates pseudo-first-order kinetics. The course of the reaction was followed by at least 80% of the reaction.

3. Results and discussion

3.1. Metal nanoparticles characterization results

Formation of AgNPs was confirmed by the color change of the solution into yellowish brown as Fig. 1A and B. The maximum absorption spectra of yellowish brown colloids are observed at 433 nm, confirms the formation of AgNPs [38]. The reduction of silver ions occurs immediately after the addition of neem leaf broth into silver nitrate solution and intensity of absorption peak increases with increasing the reaction time and reaches the maximum at time 30 min. After 24 h there are no changes in spectra of AgNPs as Fig. 1B.

The synthesized AgNPs are spherical in shape with average size 9 nm was confirmed by TEM analysis (Fig. 2A). TEM results also show the biosynthesized silver

https://doi.org/10.1016/j.heliyon.2019.e01356

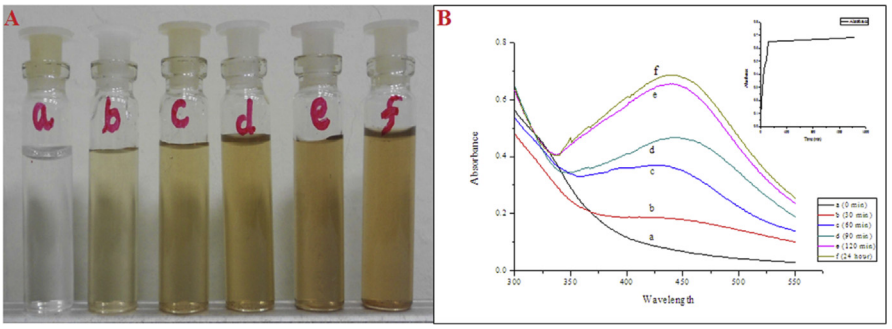

Fig. 1. (A) The time evolution of the dispersion photographs and (B) UV−vis spectra during the synthesis process (in inset Respective plot of absorbance at $\lambda_{max} = 433$ nm versus time).

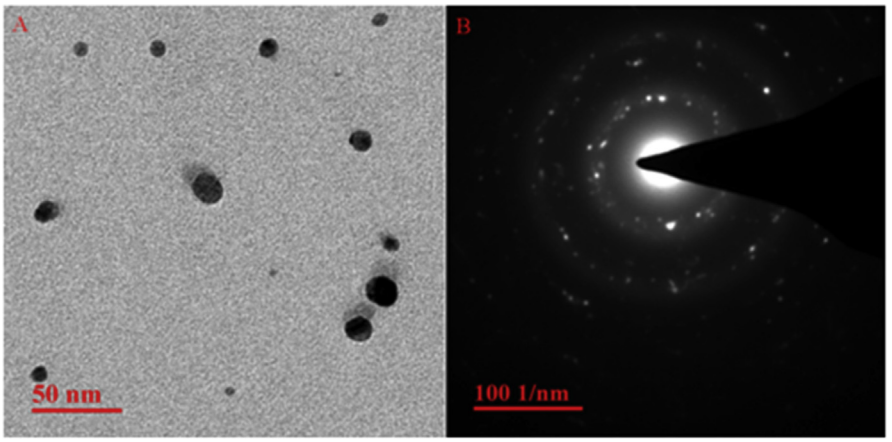

Fig. 2. (A) TEM image of synthesized Silver Nanoparticles, (B) SAED pattern of Silver Nanoparticles.

nanoparticles are surrounded by a thin layer of some capping material, thus were stable four weeks [38]. The ring-like diffraction pattern recorded by selected area electron diffraction (SAED) indicates that the particles are crystalline (Fig. 2B). Similar results are reported by the Jae Yong Song [39] for *Diopyras kaki* leaf broth synthesized AgNPs.

The XRD of AgNPs after drying NPs at 70 °C in vacuum for 12 h (Fig. 3) indicates four sharp peaks at $2\theta = 37.63$, 44.70, 64.39 and 77.20 corresponding to (111), (200), (220) and (311) representing the face centred cubic (FCC) structure. The results are matched with JCPDS No. 89-3722 and confirm the crystalline nature of AgNPs [40]. Debye-Scherrer formula gives the average size (9 nm) of AgNPs.

Size distribution of nanoparticles is also confirmed by Dynamic light scattering (DLS) (Fig. 4), results give information about the size of AgNPs between 5 to 48 nm range with average particle size 9 nm of AgNPs.

FTIR measurements give the information about the potential functional groups of the biomolecules present in leaf broth of *Azadirachta indica* (neem). FTIR spectra of

https://doi.org/10.1016/j.heliyon.2019.e01356

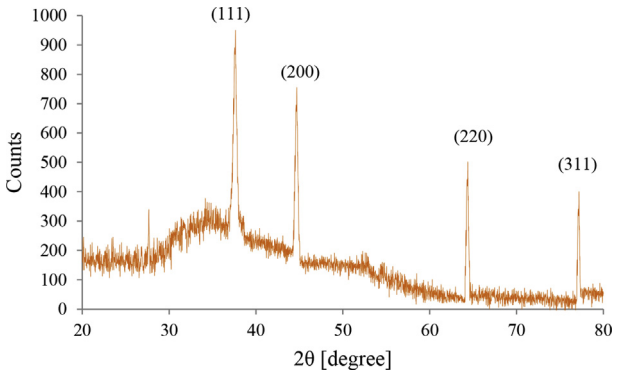

Fig. 3. XRD of biosynthesized Silver Nanoparticles.

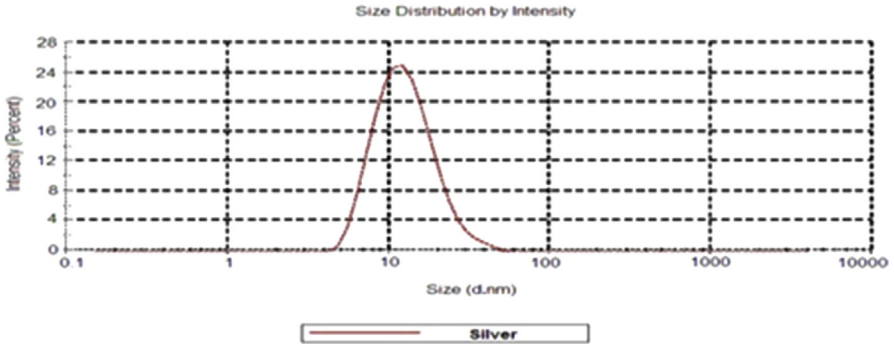

Fig. 4. Particles size distribution of synthesized Silver Nanoparticles.

synthesized nanoparticles and pure neem leaf broth are given in Fig. 5A and B respectively. The observed peak at 1609 cm^{-1}, 1381cm^{-1}, 1077 cm^{-1} in Fig. 5A are characteristics of flavanones and terpenoids that are abundant in neem plant broth [38]. The peak observed at 1609 cm^{-1} indicating C=C groups, 1381 cm^{-1} occurring to the germinal methyls and 1077 cm^{-1} are shows ether linkages, suggest the presence of flavanones or terpenoids adsorbed on the surface of AgNPs. These reducing sugars could be responsible for the reduction of silver ions into AgNPs. Terpenoids are assumed to be the surface active molecules stabilizing the nanoparticles and reduction of the metal ions is possibly facilitated by reducing sugars or terpenoids present in neem leaf broth [41].

The stability of AgNPs is also confirmed by the value of zeta potential. The obtained value is -22.4 mV (Fig. 6) suggested that the AgNPs was negatively charged in dispersed medium, so particles repel each other which prevent from aggregation.

The effect of leaf broth concentration on synthesis rate and particle size of nanoparticles was investigated. Fig. 7 shows that the time course of AgNPs formation with different neem leaf broth percentage (5%−15%) at fixed concentration of $AgNO_3$

https://doi.org/10.1016/j.heliyon.2019.e01356

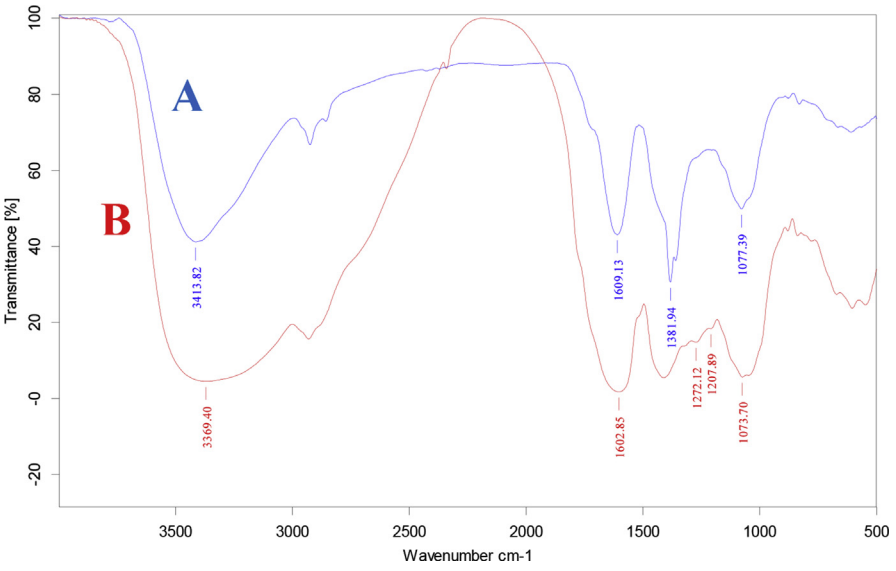

Fig. 5. Comparative FTIR spectra of (A) Synthesized AgNPs and (B) Neem leaf broth.

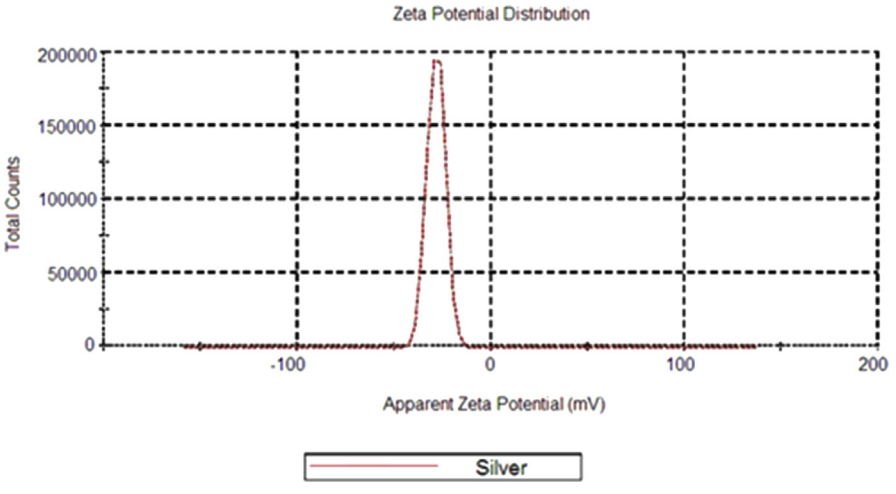

Fig. 6. Zeta potential of synthesized silver nanoparticles.

(1×10^{-3} mol dm^{-3}) on 30 °C temperature. At low percentage (5%) of leaf broth was used, a weak absorption peak obtained at 433 nm, due to the insufficient reduction of silver ions. As percentage of leaf broth increases up to 10%, the intensity of absorption peak at 433 nm also increases after that increases in percentage of neem leaf broth the absorption peak becomes lower, due to the agglomeration of AgNPs. At different leaf broth percentage the SEM images of synthesized AgNPs (Fig. 8) indicates that particle size decreases upto 10% leaf broth percentage after that size increases with increase in percentage of leaf broth, suggesting that too many reducing agents cause aggregation of the synthesized AgNPs [42].

https://doi.org/10.1016/j.heliyon.2019.e01356

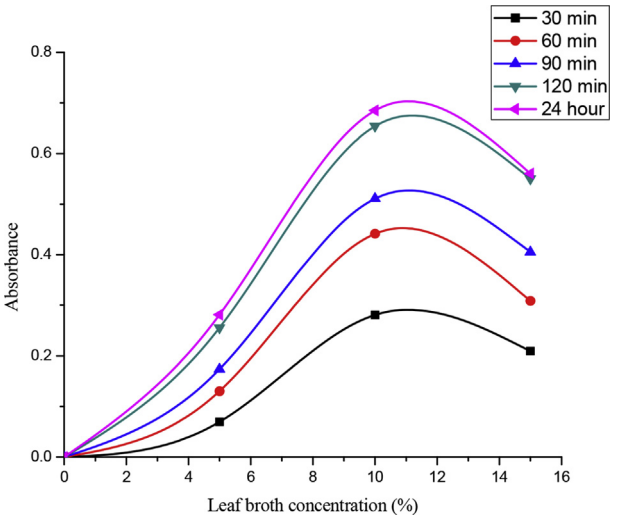

Fig. 7. Time course of AgNPs synthesis with different leaf broth concentration (5%−15%), AgNO3 = 1 × 10^{-3} mol dm^{-3}, temperature = 30 °C.

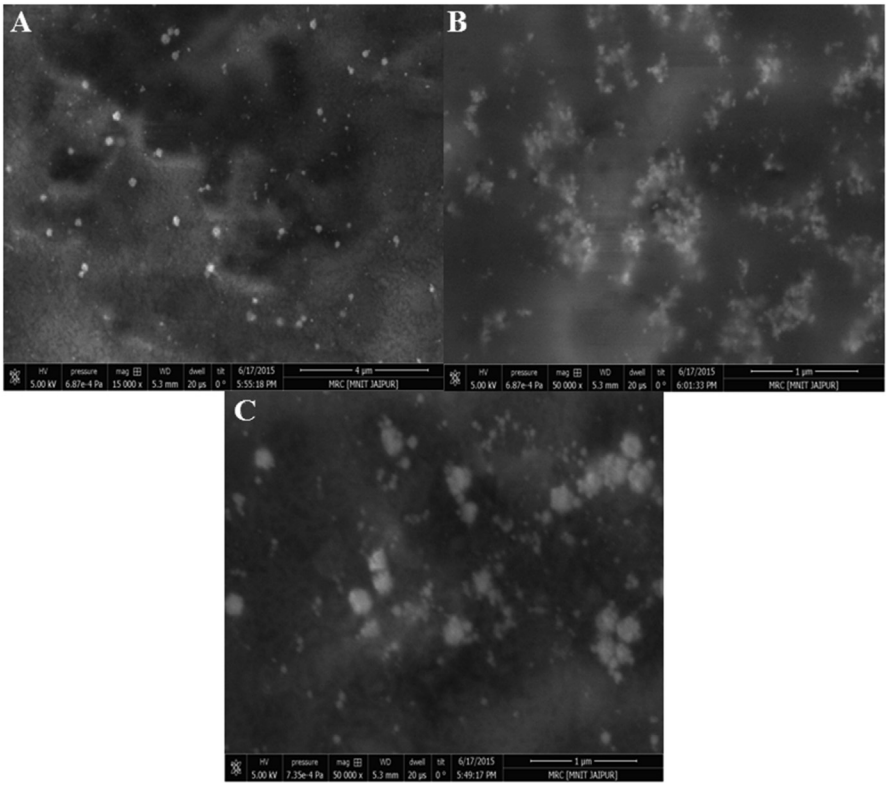

Fig. 8. SEM images of synthesized silver nanoparticles at different neem leaf broh concentration (A) 5%, (B) 10%, (C) 15%.

https://doi.org/10.1016/j.heliyon.2019.e01356

3.2. Product analysis

3.2.1. Determination of degradation products

The formed intermediates of MO during advanced oxidation process were inferred by analysing the samples with LC−MS analysis at the different time interval. Fig. 9 show that the major peaks present at the different time interval of degradation with corresponding m/z values 304, 276, 292, 156, 80, 62. After 15 min of degradation, the new peak of successive demethylated product (m/z 276) of MO was found (Fig. 9B). Furthermore, after 30 min the degradation of MO proceed, a new peak observed at m/z 292, which can attribute monohydroxylation of the aromatic ring at the ortho position of $-NH_2$ group (Fig. 9C). After that the compound m/z 292 fragmented into the compound at m/z 228 and 156 respectively then finally change into end products (CO_2, H_2O, NO_3^-, and O_3S^-) (Fig. 9D) [43].

3.2.2. UV-visible spectra of intermediates and degradation pathway

The UV-visible spectra of MO (Fig. 10A) and MO degradation with m/z values 304, 276, 292 evaluate on the basis of $[M-H]^-$ ions of the MO (Fig. 10B). The absorption

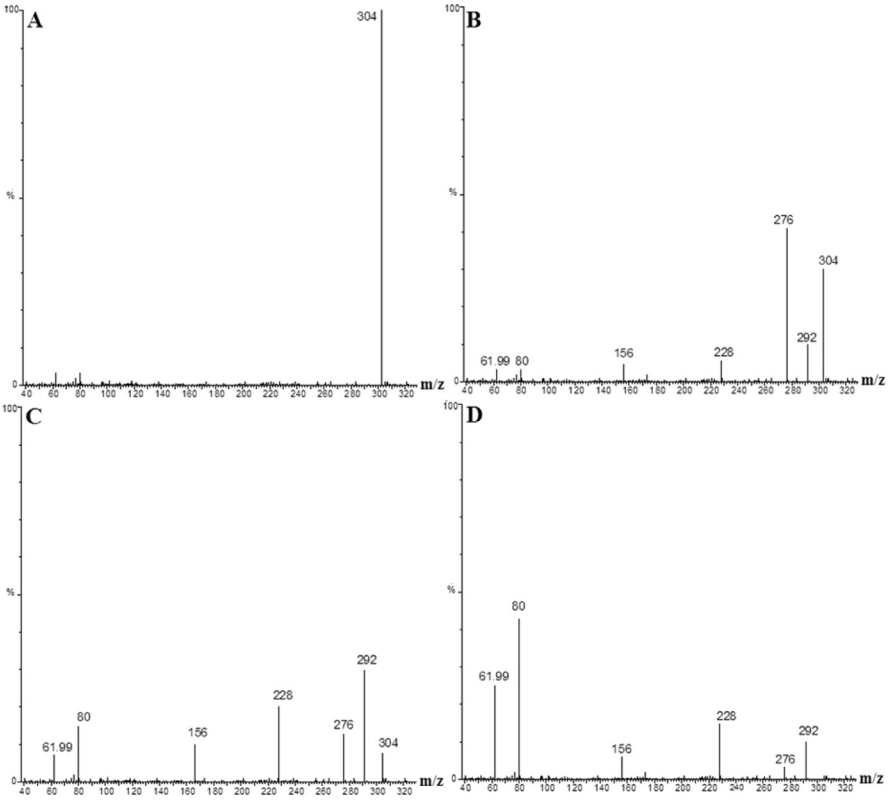

Fig. 9. LC-MS of MO degraded in AgNPs/PDS system at (A) 0 min, (B) 15 min, (C) 30 min, (D) 45 min.

https://doi.org/10.1016/j.heliyon.2019.e01356

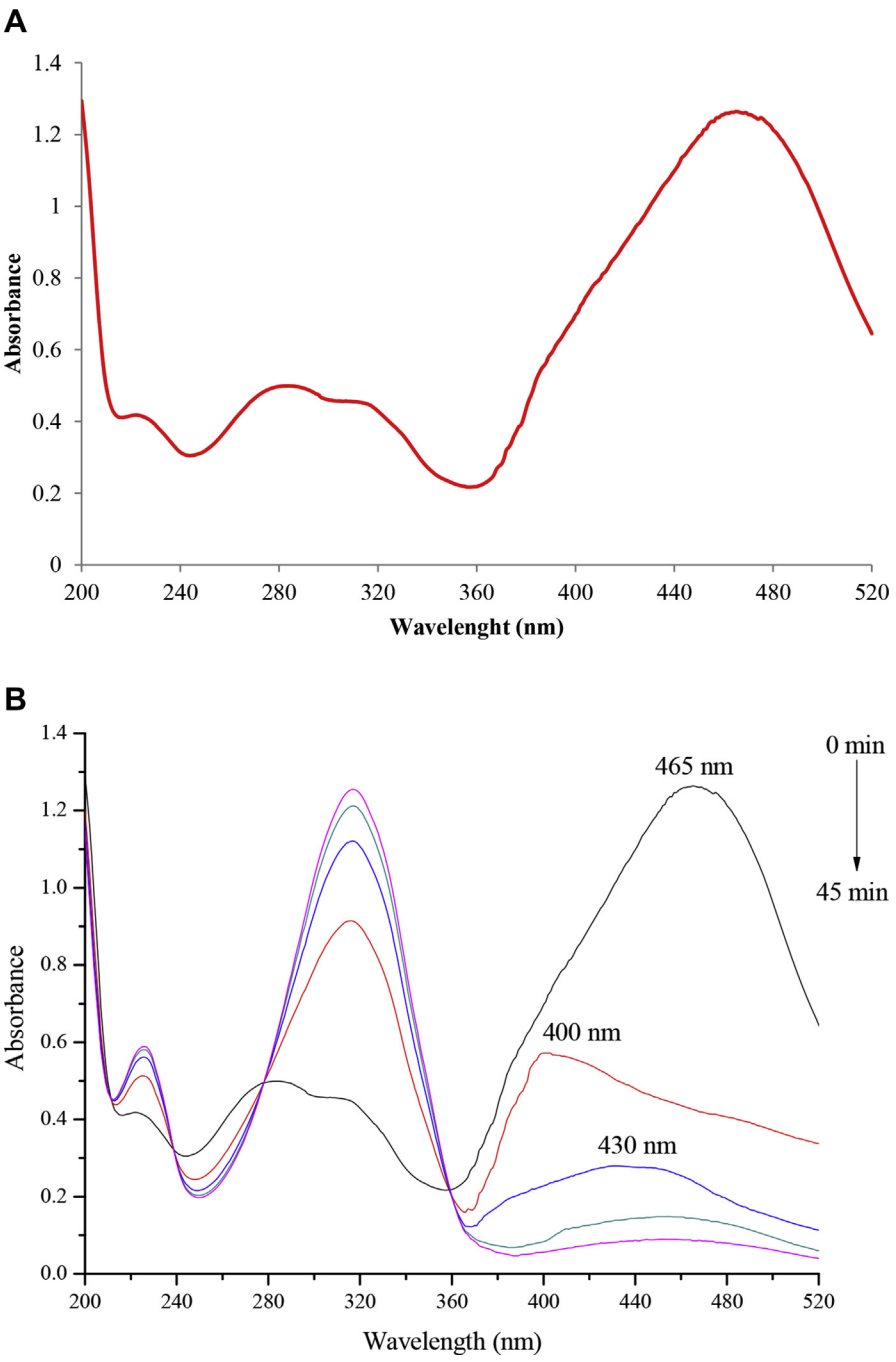

Fig. 10. (A) UV-Visible spectra of Methyl Orange (λ_{max} = 465 nm). **(B)** UV−Visible adsorption spectra of MO in AgNPs/PDS system with reaction time. ([PDS] = 5×10^{-4} mol dm^{-3}, [Dye] = 5×10^{-5} mol dm^{-3}, [AgNPs] = 1×10^{-8} mol dm^{-3}, pH = 6.5 and Temperature 30 °C).

of the extended aromatic ring and chromophore group of MO obtained at 465 nm and the additional band obtained at 271 nm are due to the presence of the aromatic ring in MO molecule (m/z 304). As the degradation proceeded, due to the successive demethylation with m/z value 276 shows a blue shift (400 nm) of the spectrum may

https://doi.org/10.1016/j.heliyon.2019.e01356

be attributed to the homolytic cleavage of the nitrogen-carbon bond, resulting in the substitution of the methyl group by the hydrogen atom. Afterward, hydroxyl radical inserted in benzene ring at the ortho position of $-NH_2$ group (m/z 292) could lead to significant wavelength redshift (430 nm). Finally, polyaromatic ring present in MO convert into monosubstituted aromatic ring and end products, it is confirmed by the presence of two new peaks at 225 nm and 323 nm in UV-visible spectra (Fig. 10B) [44]. According to these results the following degradation pathway of MO was proposed (Fig. 11).

3.3. Peroxodisulfate dependence

The AgNPs catalysed oxidative degradation of MO was studied at different concentration of PDS from 1×10^{-4} to 1×10^{-3} mol dm^{-3} at 30 °C temperature, fixed concentration of [Dye] $= 5 \times 10^{-5}$ mol dm^{-3}, [AgNPs] $= 1 \times 10^{-8}$ mol dm^{-3} and pH $= 6.5$ (Fig. 12). The rate of dye degradation increased with increase the

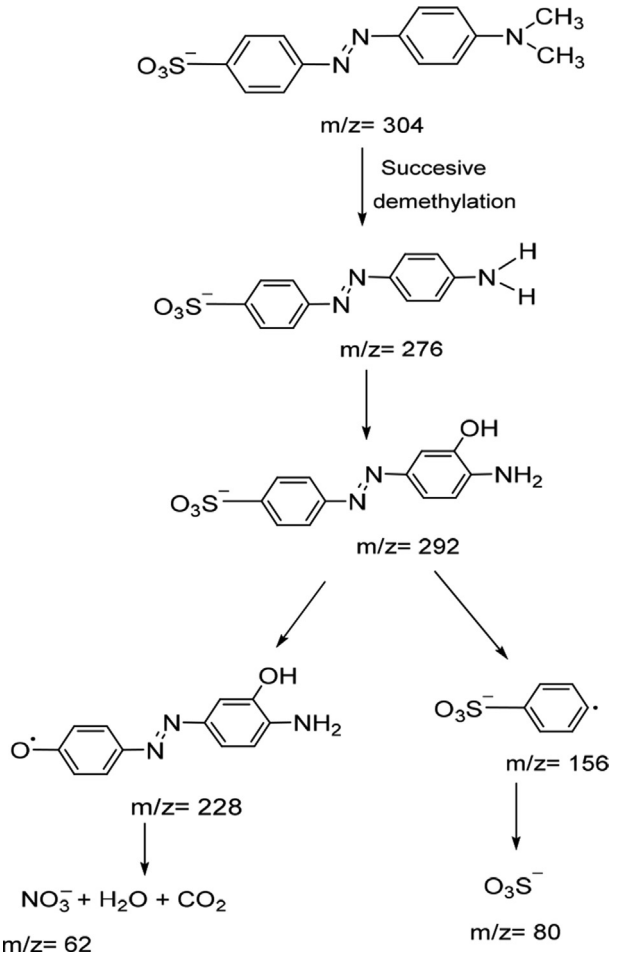

Fig. 11. Proposed degradation pathway of MO in AgNPs/PDS system.

https://doi.org/10.1016/j.heliyon.2019.e01356

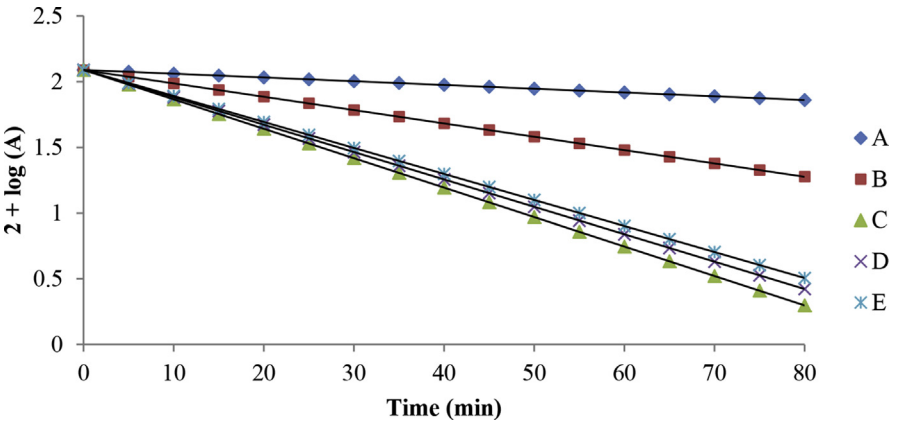

Fig. 12. Effect of variation of [PDS] at fixed [Dye] = 5.0×10^{-5} mol dm^{-3}, [AgNPs] = 1.0×10^{-8} mol dm^{-3}, pH = 6.5 and Temperature 30 °C. [PDS] (mol dm^{-3}) = (A) 1.0×10^{-4}, (B) 2.5×10^{-4}, (C) 5.0×10^{-4}, (D) 7.5×10^{-4}, (E) 10.0×10^{-4}.

initial concentration of PDS. This is likely because $SO_4^{\bullet -}$ radical ions were generated simultaneously, which in turn increases the rate of oxidation of Ag° to Ag^+ ion, Successive the oxidative decolourization of MO occurs. Furthermore, the PDS concentration increases beyond 5×10^{-4} mol dm^{-3}, the degradation rate of MO slowed down slightly. It may be due to the higher concentration of PDS the side reaction between persulfate anion ($S_2O_8^{2-}$) and $SO_4^{\bullet -}$ become more significant, which would consume more PDS, hence the remaining percentage of PDS decreases with the increases of PDS concentration (Table 1) [45].

3.4. Dye dependence

The Reaction was carried out at a constant concentration of other reactants and by varying the initial concentration of MO from 1×10^{-5} to 1×10^{-4} mol dm^{-3} at 30 °C temperature. The results indicate the degradation rate increased up to increase in 5×10^{-5} mol dm^{-3} concentration of dye after that rate decreased with an increase in dye concentration (Table 1). It may be at a constant concentration of PDS, the availability of $SO_4^{\bullet -}$ radicals are not sufficient to degrade dye molecules at higher concentration [24].

3.5. Effect of pH

The initial pH of the solution is a key factor which affects the degradation of dye because pH influences the surface charge properties of the catalyst [46]. The degradation of dye from textile dye effluents was studied at different initial pH of solution values in the range 5−8.

When the pH is higher than 8, the AgNPs becomes negatively charged according to Eq. (1).

https://doi.org/10.1016/j.heliyon.2019.e01356

Table 1. Effect of variation of [PDS], [Dye], [AgNPs] and pH on oxidative degradation of Methyl orange in aqueous solution at 30 °C.

S. No.	10^4 [PDS] mol dm^{-3}	10^5 [Dye] mol dm^{-3}	10^8 [AgNPs] mol dm^{-3} (9 nm)	pH	10^4 K_{obs} (sec^{-1})
1	1.0	5.0	1.00	6.5	1.10
2	2.5	5.0	1.00	6.5	3.90
3	5.0	5.0	1.00	6.5	8.60
4	7.5	5.0	1.00	6.5	8.00
5	10	5.0	1.00	6.5	7.60
6	5.0	1.0	1.00	6.5	3.20
7	5.0	2.5	1.00	6.5	6.50
8	5.0	5.0	1.00	6.5	8.60
9	5.0	7.5	1.00	6.5	7.81
10	5.0	10	1.00	6.5	5.99
11	5.0	5.0	0.00	6.5	1.20
12	5.0	5.0	0.25	6.5	3.05
13	5.0	5.0	0.50	6.5	4.84
14	5.0	5.0	0.75	6.5	6.70
15	5.0	5.0	1.00	6.5	8.60
16	5.0	5.0	1.50	6.5	12.20
17	5.0	5.0	2.00	6.5	15.90
18	5.0	5.0	1.00	2.5	1.20
19	5.0	5.0	1.00	5.0	7.50
20	5.0	5.0	1.00	6.5	8.60
21	5.0	5.0	1.00	7.0	7.80
22	5.0	5.0	1.00	8.0	7.30
23	5.0	5.0	1.00	9.0	6.90
24	5.0	5.0	1.00	10.0	6.30

$$AgOH + OH^- \rightarrow H_2O + Ag^- \quad (1)$$

And at the pH is lower than 5, than AgNPs is positively charged according to Eq. (2).

$$AgOH + H^+ \rightarrow H_2O + Ag^+ \quad (2)$$

The degradation rate of MO as a function of the initial pH of the solution as shown in Fig. 13 and the results illustrate that the degradation of MO was carried out effectively at 6.5 pH. The similar results were also reported by Zhong et al., 2012 [30]. The pH value of reaction was adjusted by H_2SO_4 and NaOH solution.

https://doi.org/10.1016/j.heliyon.2019.e01356

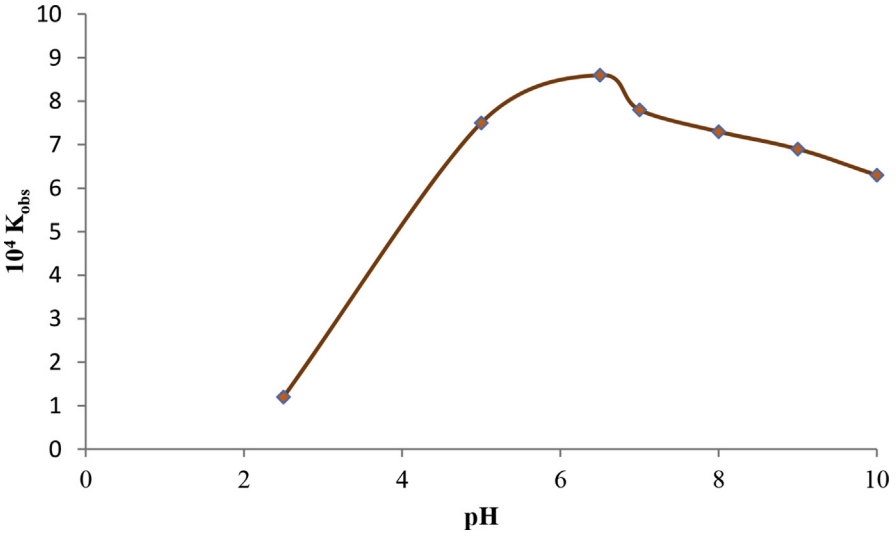

Fig. 13. Effect of variation of pH at fixed [Dye] = 5×10^{-5} mol dm^{-3}, [PDS] = 5×10^{-4} mol dm^{-3}, [AgNPs] = 1×10^{-8} mol dm^{-3} and Temperature 30 °C.

3.6. Silver nanoparticles dependence

The catalytic activity of synthesised AgNPs was evaluate in oxidative degradation of MO by PDS by varying concentration from 0.25×10^{-8} to 2.0×10^{-8} mol dm^{-3} at fixed [PDS] = 5×10^{-4} mol dm^{-3}, [Dye] = 5×10^{-5} mol dm^{-3}, pH = 6.5 and 30 °C temperature. The rate of reaction increases with increasing concentration of AgNPs [47]. In presence of small concentration (1.0×10^{-8} mol dm^{-3}) of AgNPs the degradation rate is seven times faster than in absence of AgNPs (Fig. 14) (Table

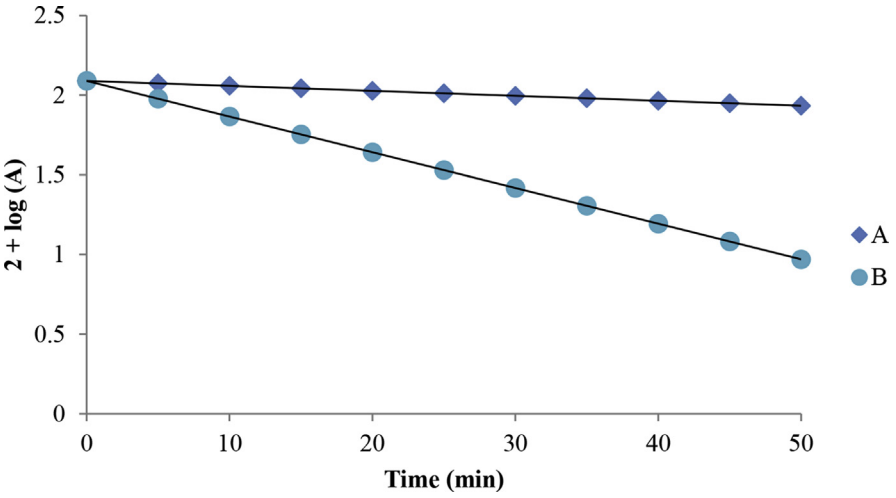

Fig. 14. Oxidative degradation of Methyl Orange by advanced oxidation process at fixed [Dye] = 5.0×10^{-5} mol L^{-1}, [PDS] = 5.0×10^{-4} mol L^{-1}, pH = 6.5 and Temperature 30 °C (A) Without catalyst, (B) With catalyst ([AgNPs] = 1.0×10^{-8} mol L^{-1}).

https://doi.org/10.1016/j.heliyon.2019.e01356

1). The catalytic activity of AgNPs also tested on real wastewater samples, were collected from drains of three different local textile industries of Kota region. Catalytic oxidative degradation was performed with a similar method as mentioned above at a different concentration of AgNPs (Fig. 15). The difference between the rate constants of sample dye and wastewater samples can be explained on the basis of structural difference and concentrations of different dye molecules present in the real wastewater samples.

3.7. Mechanism

$K_2S_2O_8$ can be activated by Ag° to generate $SO_4^{\bullet -}$ at ambient temperature. The plausible mechanism in support of the observed kinetics as given below−

$$\begin{array}{l} S_2O_8^{2-} + Ag^\circ \rightarrow SO_4^{\bullet -} + SO_4^{2-} + Ag(I) \\ \underline{SO_4^{\bullet -} + Ag(I) + Dye \rightarrow \Pr oduct + Ag^\circ} \\ S_2O_8^{2-} + Dye \xrightarrow{Ag^\circ} \Pr oduct + SO_4^{2-} \end{array}$$

Based on the results it may be concluded that the oxidative degradation of dye in presence of AgNPs by $K_2S_2O_8$ is radical ion based mechanism and the main radical ion species generated during the catalytic activation of $K_2S_2O_8$ was sulphate radical ions ($SO_4^{\bullet -}$). The role of the catalyst as a mediator for the electron transfer to PDS was also reported [32, 48, 49].

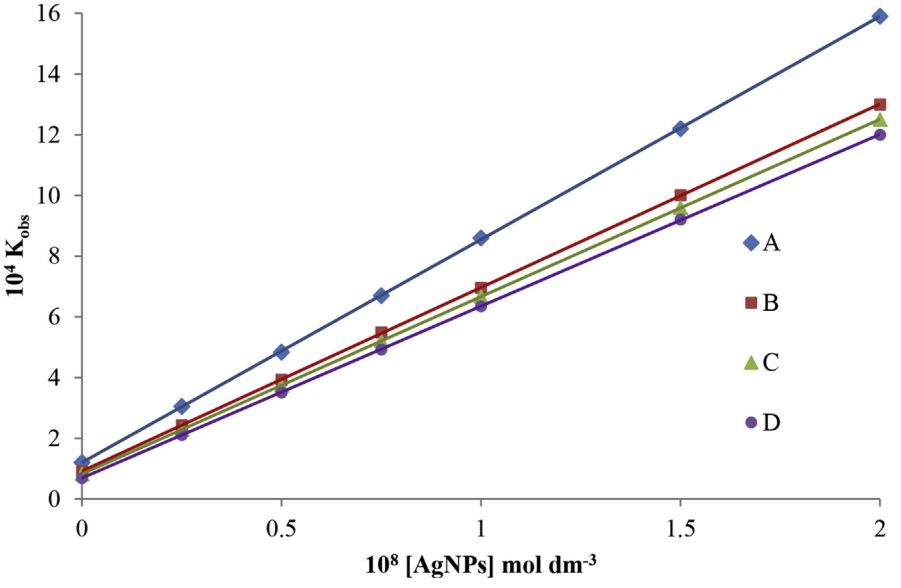

Fig. 15. Effect of [AgNPs] on degradation rate of different water samples at fixed [PDS] = 5×10^{-4} mol dm^{-3}, Temperature 30 °C. (A) Pure Methyl Orange (pH = 6.5), (B) Shopping Centre, Kota (pH = 7.2), (C) Ghantaghar, Kota (pH = 6.8), (D) Vigyan nagar, Kota (pH = 6.2).

https://doi.org/10.1016/j.heliyon.2019.e01356

Table 2. Experimental results of BOD and COD before and after advanced oxidation process.

Samples	Before AOP treatment				After AOP treatment				% BOD increases	% COD reduction
	pH	BOD (mg/l)	COD (mg/l)	BOD/ COD	pH	BOD (mg/l)	COD (mg/l)	BOD/ COD		
MO	6.5	5	70	0.07	6.3	11	28	0.39	120 %	60.0 %
Sample 1	7.0	87	486	0.18	6.8	100	212	0.47	14.9 %	56.3 %
Sample 2	6.8	58	370	0.15	6.6	80	140	0.57	37.9 %	62.0 %
Sample 3	6.2	72	410	0.17	6.0	91	168	0.54	26.3 %	59.0 %

3.8. Biodegradability

The concentration of wastewater samples was characterized by BOD and COD. The COD analysis simply indicates the total waste load in a textile waste effluent and the ratio of BOD and COD gives information about biodegradability of wastewater samples [50]. Table 2 shows BOD and COD analysis of MO dye, wastewater samples; before and after AOP treatment. The results indicate that after applying AOP treatment on MO dye, real wastewater samples; COD decreases from 56-62 % and BOD increases 14−120 %, so the value of biodegradability index increases (above 0.3). Jamil et al. 2011 [51] also reported that the value of biodegradability index less than 0.3 shows poor biodegradability in wastewater.

4. Conclusion

The present study reports highly stable, monodispersed, spherical AgNPs synthesized by the *Azadirachta indica* (neem) leaf broth as an efficient, ecofriendly and cost effective reducing and capping agent. The green synthesised AgNPs were applied as a catalyst for oxidative degradation of MO and wastewater samples in aqueous solution. The silver nanoparticles exhibited good efficiency for activation of PDS to provide sulphate radicals for degrading MO dye and real wastewater samples. Increasing catalyst and PDS concentration increase the rate of MO degradation. The results suggested that silver nanoparticles have a strong potential for fast dye degradation technologies. After AOP treatment of wastewater samples, biodegradability index is an increase, so that organic matter can be decomposed easily.

Declarations

Author contribution statement

Vijay Devra, Niharika Nagar: Conceived and designed the experiments; Performed the experiments; Analyzed and interpreted the data; Contributed reagents, materials, analysis tools or data; Wrote the paper.

https://doi.org/10.1016/j.heliyon.2019.e01356

Funding statement

Niharika Nagar was supported by University Grants Commission, India as JRF (Ref. No: 22/12/2013 (ii) EU-V).

Competing interest statement

The authors declare no conflict of interest.

Additional information

Supplementary content related to this article has been published online at https://doi.org/10.1016/j.heliyon.2019.e01356.

References

[1] V.K. Gupta, A. Nayak, S. Agarwal, Bioadsorbents for remediation of heavy metals: current status and their future prospects, Environ. Eng. Res. 20 (2015) 1−18.

[2] D. Robati, B. Mirza, M. Rajabi, O. Moradi, I. Tyagi, S. Agarwal, V.K. Gupta, Removal of hazardous Dyes-BR 12 and methyl orange using graphene oxide as an adsorbent from aqueous phase, Chem. Eng. J. 284 (2016) 687−697.

[3] T. Kamal, Y. Anwar, S.B. Khan, M. Tariq, S. Chani, A.M. Asiri, Dye adsorption and bactericidal properties of TiO_2/chitosan coating layer, Carbohydr. Polym. 148 (2016) 153−160.

[4] S.A. Khan, S.B. Khan, T. Kamal, M. Yasir, A.M. Asiri, Antibacterial nanocomposites based on chitosan/Co-MCM as a selective and efficient adsorbent for organic dyes, Int. J. Biol. Macromol. 91 (2016) 744−751.

[5] A. Ahmad, A. Idris, B. Hameed, Color and COD reduction from cotton textile processing wastewater by activated carbon derived from solid waste in column mode, Desalin. Water Treat. 41 (2012) 224−231.

[6] A.L. Ahmad, W.A. Harris, B.S. Ooi, Removal of dye from wastewater of textile industry using membrane technology, Journal Teknologi 36 (2012) 31−44.

[7] I. Arslan-Alaton, J.L. Ferry, Application of polyoxotungstates as environmental catalysts: wet air oxidation of acid dye Orange II, Dyes Pigments 54 (2002) 25−36.

[8] Z.H. Wang, W.H. Ma, C.C. Cheng, J.C. Zhao, Light-assisted decomposition of dyes over iron-bearing soil clays in the presence of H_2O_2, J. Hazard Mater. 168 (2009) 1246−1252.

[9] V.K. Gupta, R. Jain, A. Nayak, S. Agarwal, M. Shrivastava, Removal of the hazardous dye—tartrazine by photodegradation on titanium dioxide surface, Mater. Sci. Eng. C 31 (2011) 1062−1067.

[10] S. Karthikeyan, V.K. Gupta, R. Boopathy, A. Titus, G. Sekaran, A new approach for the degradation of high concentration of aromatic amine by heterocatalytic Fenton oxidation: kinetic and spectroscopic studies, J. Mol. Liq. 173 (2012) 153−163.

[11] S.K. Ling, S.-B. Wang, Y.-L. Peng, Oxidative degradation of dyes in water using Co^{2+}/H_2O_2 and Co^{2+}/peroxymonosulfate, J. Hazard Mater. 178 (2010) 385−389.

[12] P.R. Shukla, S.-B. Wang, H.M. Ang, M.O. Tadé, Photocatalytic oxidation of phenolic compounds using zinc oxide and sulphate radicals under artificial solar light, Separ. Purif. Technol. 30 (2010) 338−344.

[13] K.H. Chan, W. Chu, Degradation of atrazine by cobalt-mediated activation of peroxymonosulfate: different cobalt counteranions in homogenous process and cobalt oxide catalysts in photolytic heterogeneous process, Water Res. 43 (2009) 2513−2521.

[14] X.-Y. Chen, J.-W. Chen, X.-L. Qiao, D.-G. Wang, X.-Y. Cai, Performance of nano-Co_3O_4/peroxymonosulfate system: kinetics and mechanism study using Acid Orange 7 as a model compound, Appl. Catal. B Environ. 80 (2008) 116−121.

[15] E. Psillakis, D. Mantzavinos, Enhancement of biodegradability of industrial wastewaters by chemical oxidation pre-treatement, J. Chem. Technol. Biotechnol. 79 (2004) 431−454.

[16] H.S. Devi, T.D. Singh, Synthesis of copper oxide nanoparticles by a novel method and its Apllication in the degradation of methyl orange, Adv. Electron. Elec. Eng. 4 (2014) 83−88. ISSN 2231-1297.

[17] R. Saravanan, E. Sacari, F. Gracia, M.M. Khan, E. Mosquera, V.K. Gupta, Conducting PANI stimulated ZnO system for visible light photocatalytic degradation of coloured dyes, J. Mol. Liq. 221 (2016) 1029−1033.

[18] A. Asfaram, M. Ghaedi, S. Agarwal, I. Tyagi, V.K. Gupta, Removal of basic dye Auramine-O by ZnS: Cu nanoparticles loaded on activated carbon Optimization of parameters using response surface methodology with central composite design, RSC Adv. 5 (2015) 18438−18450.

[19] I. Ahmad, T. Kamal, S.B. Khan, A.M. Asiri, An efficient and easily retrievable dip catalyst based on silver nanoparticles/chitosan-coated cellulose filter paper, Cellulose 23 (2016) 3577−3588.

https://doi.org/10.1016/j.heliyon.2019.e01356

[20] F. Ali, S.B. Khan, T. Kamal, Y. Anwar, K.A. Alamry, A.M. Asiri, Bactericidal and catalytic performance of green nanocomposite based on chitosan/carbon black fiber supported monometallic and bimetallic nanoparticles, Chemosphere 188 (2017) 588–598.

[21] A.A. Firooz, A.R. Mahjoub, A. Khodadadi, Hydrothermal synthesis of ZnO/SnO_2 nanoparticles with high photocatalytic activity, World Acad. Sci. Eng. Technol. 5 (2011) 118–120. ISNI:0000000091950263.

[22] R.A. Soomro, S.T.H. Sherazi, Sirajuddin, N. Memon, M.R. Shah, N.H. Kalwar, K.R. Hallam, A. Shah, Synthesis of air stable copper nanoparticles and their use in catalysis, Adv. Mat. Lett. 5 (2014) 191–198.

[23] A. Goel, R. Bhatt, Neetu, kinetic studies on nanocatalysis by iridium nanoclusters in some oxidation reactions, Int. J. Res. Chem. Environ. 2 (2012) 210–217. ISSN 2248-9649.

[24] N. Nagar, V. Devra, Activation of peroxodisulphate and peromonosulfate by greeen synthesized copper nanoparticles for Methyl Orange degradation: a kinetic study, J. Environ. Chem. Eng. 5 (2017) 5793–5800.

[25] N. Nagar, V. Devra, Oxidative degradation of Orange G by peroxomonosulfate in presence of biosynthesized copper nanoparticles - a kinetic study, Environmental Technology & Innovation 10 (2018) 281–289.

[26] S.S. Shankar, A. Rai, A. Ahmad, M. Sastry, Rapid synthesis of Au, Ag, and bimetallic Au core Ag shell nanoparticles using Neem (*Azadirachta indica*) leaf broth, J. Colloid Interface Sci. 275 (2004) 496–502.

[27] A. Yeganeh-Faal, M. Bordbar, N. Negahdar, M. Nasrollahzadeh, Green synthesis of the Ag/ZnO nanocomposite using *Valeriana officinalis L.* root extract: application as a reusable catalyst for the reduction of organic dyes in a very short time, IET Nanobiotechnol. 11 (2017) 669–676.

[28] M. Maryami, M. Nasrollahzadeh, E. Mehdipour, S.M. Sajadi, Preparation of the Ag/RGO nanocomposite by use of *Abutilon hirtum* leaf extract: a recoverable catalyst for the reduction of organic dyes in aqueous medium at room temperature, Int. J. Hydrogen Energy 41 (2016) 21236–21245.

[29] M. Maham, M. Nasrollahzadeh, M. Nekoei, Biosynthesis of Ag/reduced graphene oxide/$Fe_{[3]}O_{[4]}$ using *Lotus garcinii* leaf extract and its application as a recyclable nanocatalyst for the reduction of 4-nitrophenol and organic dyes, J. Colloid Interface Sci. 497 (2017) 33–42.

https://doi.org/10.1016/j.heliyon.2019.e01356

[30] J.B. Zhong, J.Z. Li, Y. Lu, S.T. Huang, W. Hu, Oxidation of methyl orange solution with potassium peroxydisulfate, Iran. J. Chem. Chem. Eng. 31 (2012) 21−24. ISSN 1021-9986.

[31] M.H. Rasouliard, R. Marani, H. Majidzadeh, I. Baheri, Ultraviolet light-emitting diodes and peroxydisulfate for degradation of basic red 46 from contaminated water, Environ. Eng. Sci. 28 (2011) 229−235.

[32] L. Hou, H. Zhang, X. Xue, Ultrasound enhancd heterogeneous activation of peroxydisulfate by magnetite catalyst for the degradation of tetracycline in water, Separ. Purif. Technol. 84 (2012) 147−152.

[33] A. Hatamifard, M. Nasrollahzadeh, S.M. Sajadi, Biosynthesis, characterization and catalytic activity of an Ag/zeolite nanocomposite for base- and ligand-free oxidative hydroxylation of phenylboronic acid and reduction of a variety of dyes at room temperature, New J. Chem. 40 (2016) 2501−2513.

[34] B. Khodadadi, M. Bordbar, A. Yeganeh-Faal, M. Nasrollahzadeh, Green synthesis of Ag nanoparticles/clinoptilolite using Vaccinium macrocarpon fruit extract and its excellent catalytic activity for reduction of organic dyes, J. Alloy. Comp. 719 (2017) 82−88.

[35] B. Khodadadi, M. Bordbar, M. Nasrollahzadeh, *Achillea millefolium* L. extract mediated green synthesis of waste peach kernel shell supported silver nanoparticles: application of the nanoparticles for catalytic reduction of a variety of dyes in water, J. Colloid Interface Sci. 493 (2017) 85−93.

[36] N. Nagar, S. Jain, P. Kachhawah, V. Devra, Synthesis and characterization of silver nanoparticles via green route, Kor. J. Chem. Eng. 33 (2016) 2990−2997.

[37] L. Obeid, A. Bée, D. Talbot, S.B. Jaafar, V. Dupuis, S. Abramson, V. Cabuil, M. Welschbillig, Chitosan/maghemite composite: a magsorbent for the adsorption of methyl orange, J. Colloid Interface Sci. 410 (2013) 52−58.

[38] P. Banerjee, M. Satapathy, A. Mukhopahayay, P. Das, Leaf extract mediated green synthesis of silver nanoparticles from widely available Indian plants: synthesis, characterization, antimicrobial property and toxicity analysis, Bioresourc. Bioprocess. 1 (2014) 1−10.

[39] J.Y. Song, B.S. Kim, Rapid biological synthesis of silver nanoparticles using plant leaf extracts, Bioproc. Biosyst. Eng. 32 (2009) 79−84.

[40] K. Anandalakshmi, J. Venugobal, V. Ramasamy, Characterization of silver nanoparticles by green synthesis method using *Pedalium murex* leaf extract and their antibacterial activity, Appl. Nanosci. 6 (2016) 399−408.

 https://doi.org/10.1016/j.heliyon.2019.e01356

[41] N. Nagar, V. Devra, Green synthesis and characterization of copper nanoparticles using Azadiracta indica leaves, Mater. Chem. Phys. 213 (2018) 44−51.

[42] M. Vanaja, K. Paulkumar, M. Baburaja, S. Rajeshkumar, G. Gnanajobitha, C. Malarkodi, M. Sivakavinesan, G. Annadurai, Degradation of Methylene Blue using biologically synthesized silver nanoparticles, Bioinorgan. Chem. Appl. 2014 (8) (2014), 742346.

[43] S. Hisaindee, M.A. Meetani, M.A. Rauf, Application of LC-MS to the analysis of advanced oxidation process (AOP) degradation of dye products and reaction mechanisms, TrAC Trends Anal. Chem. 49 (2013) 31−44.

[44] T. Chen, Y. Zheng, J.−M. Lin, G. Chen, Study on the photocatalytic degradation of methyl orange in water using Ag/ZnO as catalyst by liquid chromatography electrospray ionization ion-trap mass spectrometry, J. Am. Soc. Mass Spectrom. 19 (2008) 997−1003.

[45] J. Wu, H. Zhang, J. Qiu, Degradation of Acid Orange 7 in aqueous solution by a novel electro/Fe^{2+}/peroxydisulfate process, J. Hazard Mater. 215−216 (2012) 138−145.

[46] M.A. Behnajady, H. Eskandarloo, Preparation of TiO2 nanoparticles by the sol−gel method under different pH conditions and modeling of photocatalytic activity by artificial neural network, Res. Chem. Intermed. 41 (2013) 2001−2017.

[47] J. Santhanalakshmi, V. Dhanalakshmi, Chitosan silver nanoparticles assisted oxidation of Textile dyes with H_2O_2 aqueous solution: kinetic studies with pH and mass effect, Indian J. Sci. Technol. 5 (2012) 3834−3838. ISSN: 0974-6846.

[48] H. Lin, H. Zhng, L. Hou, Degradation of C. I. Acid orange 7 in aqueous solution by a novel electro/$Fe_{[3]}O_{[4]}$/PDS process, J. Hazard Mater. 276 (2014) 182−191.

[49] K. Govindan, M. Raja, S.U. Maheshwari, M. Noel, Analysis and understanding of amido black 10B dye degradation in aqueous solution by electrocoagulation with the conventional oxidants peroxomonosulfate, peroxodisulfate and hydrogen peroxide, Environ. Sci. Water Res. Technol. 1 (2015) 108−119.

[50] Y.Y. Choi, S.R. Baek, J.I. Kim, J.W. Choi, J. Hur, T.U. Lee, C.J. Park, B.J. Lee, Characteristics and biodegradability of wastewater organic matter in municipal wastewater treatment plants collecting domestic wastewater and industrial discharge, Water 9 (2017) 409−420.

https://doi.org/10.1016/j.heliyon.2019.e01356

[51] T.S. Jamil, M.Y. Ghaly, I.E. El-Seesy, E.R. Souaya, R.A. Nasr, A comparative study among different photochemical oxidation processes to enhance the biodegradability of paper mill wastewater, J. Hazard Mater. 185 (2011) 353–358.

https://doi.org/10.1016/j.heliyon.2019.e01356